As per UGC guidelines an electronic bar code is provided to secure your paper

International Journal for Modern Trends in Science and Technology
Volume 12, Issue 07, pages 206-218.
ISSN: 2455-3778 online
Available online at: http://www.ijmtst.com/vol12issue06.html
DOI: https://doi.org/10.5281/zenodo.21362194

Robust Noise-Resilient R-Peak Detection Algorithm for Multiscale HRV Analysis

Md Abdul Kareem | Dr. Simhadri Vadrevu

Department of Electronics and Communication Engineering, Godavari Global University, Rajahmundry, AP, India.

To Cite this Article
Md Abdul Kareem & Dr. Simhadri Vadrevu (2026). Robust Noise-Resilient R-Peak Detection Algorithm for Multiscale HRV Analysis. International Journal for Modern Trends in Science and Technology, 12(07), 206-218. https://doi.org/10.5281/zenodo.21362194

Article Info
Received: 16 June 2026; Revised: 10 July 2026; Accepted: 13 July 2026.

Copyright © The Authors ; This is an open access article distributed under the Creative Commons Attribution License, which permits unrestricted use, distribution, and reproduction in any medium, provided the original work is properly cited.

KEYWORDS

ECG, R-peak detection, heart rate variability, HRV, wearable monitoring, noise-resilient detection, multiscale analysis

ABSTRACT

The Heart Rate Variability (HRV) analysis largely depends on the accurate detection of R-peaks in Electrocardiogram (ECG) signals. Particularly in wearable and real-time monitoring devices where signal quality is frequently affected by motion artifacts, muscle noise, and surrounding noises. In this work, a robust and noise-resilient R-peak approach is applied to handle such real-world disturbances effectively while supporting multiscale HRV analysis. The proposed method is analyzed using sleep ECG recordings, and the resulting time-domain HRV measures shows consistent and stable patterns among different subjects. The SDNN values range from 0.0449 ± 0.0132 s to 0.1189± 0.0139 s, while RMSSD values vary between 0.0221 ± 0.0026 s and 0.0757 ± 0.0467 s. The coefficient of variation (CVNN) is observed within 0.0542 ± 0.0154 to 0.1327 ± 0.0159. In the frequency domain, low-frequency (LF) power ranges from 0.0006± 0.0003 to 0.0070 ± 0.0020, whereas high-frequency (HF) power varies between 0.0001 ± 0.0001 and 0.0029 ± 0.0035. The LF/HF ratio spans from 0.9377 ± 0.5480 to 11.8765 ± 4.1753. The results show that the proposed algorithm continues to detect R-peaks consistently and provides physiologically meaningful HRV parameters, even when the signal is noisy. As a result, it makes suitable for long term wearable health monitoring applications.

1. INTRODUCTION

Every year, death of millions of people all around the world due to cardiovascular diseases (CVDs), is making a significant challenge to healthcare providers [1]. Thereby having an early diagnosis immediately after onset of primary symptoms and monitoring one's health to prevent serious cardiac conditions has gained significant importance in recent times [2]. There are several clinical approaches have developed for addressing heart-related conditions, among heart rate variability (HRV) being one such technique. It is considered as a non-invasive biomarker detection technique that represents the relationship between the sympathetic and parasympathetic branches of the autonomic nervous system [3]. HRV is generally obtained from electrocardiogram (ECG) signals and

offers valuable insights of heart function, body stress levels, and the activity of the human autonomic nervous system [4]. In Recent times the biomedical sensing technologies have advanced the development of wearable health devices capable of tracking physiological signals in everyday environments and in scenarios where individuals are outside healthcare facilities [5]. These wearable health devices majorly have sensors with MEMS based components, wireless communication modules, and embedded signal processing systems to get ECG signals in real time [6]. As a result, these systems support to record long-term cardiac monitoring during everyday activities and help in the early identification of cardiovascular conditions [7]. Particularly, wearable health devices that track ECG signals have attracted public attention due to their convenience, accessibility, and cost-effectiveness in providing continuous health assessment and monitoring. [8].

Even though wearable health devices are having several advantages and various technologies that offer multiple benefits to record ECG signals, they are usually affected by different kinds of noise and interference [9], such as body movement, muscle activity, baseline drift, and Power line noise, all of which can degrade the quality of the recorded ECG signal [10]. These disturbances can change the characteristics and morphology structure of ECG waveforms, making it difficult to extract accurate information and increases the difficulty of further analysis [11]. As a result, the presence of noise can reduce the effectiveness of HRV analysis and may lead to incorrect conclusions of cardiac health conditions [12]. The R-peak of the QRS complex in an ECG signal represents the highest amplitude, is crucial to accurately detect the HRV analysis [13]. These HRV parameters are derived from the time intervals of the consecutive R-peaks, which are referred as RR intervals [14]. A minor error in detection of R-peak can change results in HRV metric curves and decreases the accuracy of cardiovascular analysis [15]. Standard R-peak detection methods primarily use signal filtering, differentiation, and adaptive threshold to identify QRS complexes in ECG signals [16].

While these methods work well under normal conditions, their performance declines when used with ECG recordings collected from wearable health devices [17]. Due to which, during real-time monitoring, ECG recordings may be affected by random noise and waveform may disrupt, which impacts traditional algorithms [18]. To address these challenges related with ECG signals, researchers have implemented various advanced signal processing techniques to improve the signal quality before extracting important features for further analysis [19]. Wavelet transforms, adaptive filtering, and multiscale signal decomposition are such techniques that are used to improve the analysis of ECG signals [20]. These techniques help in separating valuable heart data from unnecessary noise while maintaining the waveform shape and pattern of the ECG signal that is necessary [21]. This QRS complexes across various frequency ranges identify multiscale analysis and improve peak detection accuracy in noisy recording conditions [22].

Recent studies show that the traditional signal processing methods are widely applied, due to increase in importance of intelligent algorithms and machine learning techniques for automated ECG analysis [23]. These data-based techniques can identify complex patterns in physiological signals, thereby improving the accuracy of cardiac event detection in large scale datasets [24]. However, if ECG signals are affected by noise or artifacts then maintaining consistent performance becomes a challenge. As a result, creating a strong algorithm that can maintain high performance in the presence of noise is a crucial need for accurate HRV analysis and real-time wearable health monitoring applications [25]. This study proposes a Robust Noise Resilient R-Peak Detection Algorithm for Multiscale HRV Analysis. The main aim of the proposed method is to improve the R-peak accuracy by combining advanced preprocessing techniques with multiscale signal analysis. Which helps to reduce noise while keeping essential ECG features and improves RR interval extraction. Thus, this framework improves HRV analysis and supports long-term cardiac monitoring in wearable health systems.

II. RELATED WORK

Modern healthcare related to ECG and HRV analysis have explained the importance of ECG-based cardiac analysis, HRV estimation, and automatic detection of heart problems mainly in wearable technologies and remote monitoring systems. Recent studies have also observed several approaches, such as using of

biomedical radar to detect atrial arrhythmias [1] along with AI models that combine compressive sensing with lightweight convolutional neural networks for accurate arrhythmia detection [2]. In addition, researchers have analyses non-contact millimetre-wave cardiography systems for continuous HRV monitoring [3]. Researchers have also examined methods for estimating HRV from photoplethysmography signals using signal transformation and recurrent learning techniques [4], and examine ECG-derived HRV features for applications like anxiety detection [5]. At the same time, deep learning and hybrid intelligence techniques have become vital for cardiac monitoring. For instance, deep learning methods are used for stress detection through ECG signals [6], while transformer-based architectures effectively predict atrial fibrillation from short ECG recordings [7]. Researchers have also studied the effect of ECG noise on ultra-short-term HRV parameters [8], revealing issues with real-world signal conditions. Further studies focus on heart rate estimation with convolutional and adversarial frameworks [9], predicting heart disease in healthcare IoT settings [10], and estimating HRV parameters from long-term wireless physiological recordings [11]. Other research has explored the potential of long-duration HRV as a wellness marker [12] and the connection between ultra-short-term HRV and atrial fibrillation in heart failure patients [13]. Several works emphasize improving signals, intelligent classification, and real-time cardiovascular monitoring. Hybrid AI frameworks with automatic gain control for ECG monitoring [14], deep learning and statistical methods for detecting cardiac arrest [15], and multi-sensor cardiovascular health monitoring systems [16] reflect the growing interest in reliable automated analysis. Likewise, hybrid CNN-based models for arrhythmia detection [17], advanced deep learning for multi-lead ECG diagnosis [18], optimized arrhythmia prediction models [19], and CNN-based panic attack detection using ECG signals [20] show the wide-ranging use of ECG-driven decision systems. Machine learning based studies such as heart disease classification have played a key role in improving cardiac analysis [21], arrhythmia related HRV detection [22], prediction of sudden cardiac death [23], heartbeat classification among patients [24], and multimodal deep learning approaches for cardiovascular risk prediction [25]. world issues like motion-related noise, muscle interference, baseline drift, and environmental disturbances. Thus, accurate detection of RR intervals is crucial for HRV analysis. Even a minor error in peak detection can impact time-domain, The frequency-domain, and nonlinear HRV measures, which affects the further analysis. These challenges state the need for a strong and noise-resistant R-peak detection system that improves ECG features while improving peak detection accuracy. This approach is essential for supporting multiscale HRV analysis in real-world monitoring settings.

III. PROPOSED METHODOLOGY

Proposed framework works to find R-peaks even in noisy ECG signals and extract meaningful multiscale HRV features from the identified heart beat locations. The complete methodology consists of four major stages: ECG preprocessing, segment-wise R-peak detection, RR-interval generation and validation, and HRV feature extraction in the time and frequency domains. A block-level description of the workflow is as follows: 1) acquisition and resampling of ECG data, 2) normalization and segment-wise peak detection, 3) refinement of candidate R-peaks using physiological constraints, and 4) computation of HRV indices from validated RR intervals. Fig. 1 shows the overall workflow of the proposed method.

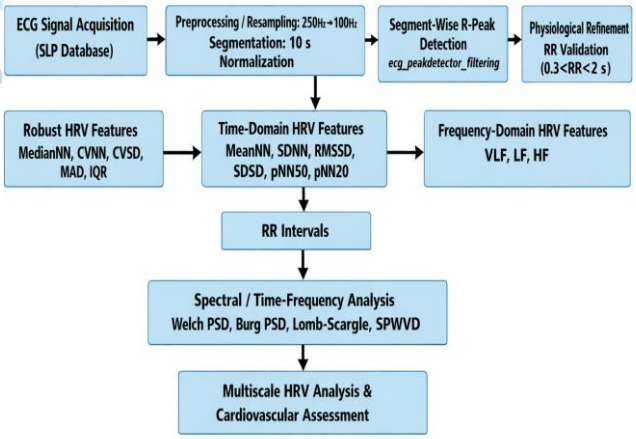

Fig. 1. Block diagram of the proposed robust noise-resilient R-peak detection and multiscale HRV analysis framework.

A.ECG Signal Acquisition and Preprocessing

The ECG recordings are obtained from the SLP database. In the implemented workflow, the original ECG signal is loaded from the database and the first channel is selected for analysis. Since the original sampling frequency is 250 Hz, the signal is resampled to 100 Hz before R-peak detection in order to reduce computational complexity while preserving the dominant morphology of the QRS complex. The analyzed ECG signal is represented as

$$x[n] = \text{resample}(s[n], 100, 250), \quad (1)$$

where s[n] denotes the original ECG sequence and x[n] denotes the resampled signal.

For localized and robust analysis, the resampled ECG is divided into fixed-duration segments of 10s each. If f_s is the working sampling frequency and T_{seg} is the segment duration, then the segment length in samples is

$$N_{Seg} = fs \times T_{Seg}. \quad (2)$$

In this work, $f_s = 100\ H_Z$ and $T_{seg} = 10_S$, so that each segment contains 1000 samples.

To reduce amplitude variability between segments, each ECG segment is normalized with respect to its maximum absolute amplitude:

$$X_n[k] = \frac{x[k]}{\max(|x[k]|)}. \quad (3)$$

This normalization stabilizes the input range and improves the consistency of subsequent peak detection across records with different amplitudes.

B.Segment-Wise R-Peak Detection

After normalization, each ECG segment is processed by the peak detection function **ecg_peakdetector_filtering**. The detector produces several intermediate outputs, corresponding to different stages of the processing chain, together with the final R-peak locations. Based on the implemented code and output visualization, the signal flow includes the normalized ECG, an intermediate transformed signal, a smoothed representation, a decision signal, approximate peak locations, and the final detected R-peaks.

Let the normalized input ECG segment be denoted by X_n [k]. A sequence of filtering and enhancement operations is applied to emphasize rapid transitions associated with QRS complexes while suppressing slow baseline variations and high-frequency disturbances. The intermediate outputs may be represented generically as

$$d[k] = F1\{x_n[k]\}, \quad (4)$$

$$s[k] = F2\{d[k]\}, \quad (5)$$

$$z[k] = F3\{s[k]\}, \quad (6)$$

where F_1 {·}, F_2 {·}, and F_3 {·} denote the internal transformation, smoothing, and enhancement stages used to expose QRS-related events. Approximate peak locations are first identified from the transformed signal, and the final R-peak positions are then selected after refinement.

If $R_{seg} = \{r_1, r_2, \ldots, r_M\}$ denotes the detected R-peak sample positions within a segment, then their absolute positions in the full ECG recording are obtained as

$$Rabs = (i-1)N_{seg} + R_{seg}, \quad (7)$$

where i denotes the segment index. The final collection of detected peaks over the complete ECG record is constructed by concatenating the segment-wise detections.

C.Physiological Refinement of Candidate Peaks

Since ECG signals acquired in wearable and ambulatory environments may contain motion artifacts and noise-induced false peaks, the candidate detections are further constrained using physiological rules. In particular, the RR intervals obtained from successive detected peaks must fall within a physiologically plausible range. If D = {d1, d2, . . ., d_N} denotes the validated R-peak sample positions, then the RR intervals are computed as

$$RR_I = di+1 - di\ \frac{di+1 - di}{fs},\ i = 1, 2, \ldots, N-1. \quad (8)$$

Only intervals satisfying,

$$0.3 < RR_i < 2.0\ s \quad (9)$$

are retained for subsequent HRV analysis. This range suppresses implausibly short intervals due to false detections and abnormally long intervals caused by missed peaks or corrupted segments. Segments with insufficient valid peaks are discarded from HRV computation.

D. Multiscale HRV Analysis

After robust R-peak localization, HRV analysis is performed on the detected peaks. The validated R-peak sequence is divided into non-overlapping segments of

duration 5 min for multiscale HRV estimation. For each segment, both conventional and robust HRV descriptors are computed

1) ***Time-Domain HRV Features:*** Let the valid NN interval sequence in a segment be

$$\{NN_1, NN_2, \ldots, NN_N\}. \quad (10)$$

The mean NN interval is given by

$$\overline{NN} = \frac{1}{N}\sum_{i=1}^{N} NN_i. \quad (11)$$

The mean heart rate is computed as

$$\text{Mean HR} = \frac{60000}{\overline{NN}}, \quad (12)$$

When $\overline{NN}$ is expressed in milliseconds.

The standard deviation of NN intervals (SDNN) is

$$\text{SDNN} = \sqrt{\frac{1}{K-1}\sum_{j=1}^{k}\left(NN_j - \overline{NN}\right)^2} \quad (13)$$

The root mean square of successive difference (RMSSD) is

$$\text{RMSSD} = \sqrt{\frac{1}{N-1}\sum_{i=1}^{N-1}(NN_{i+1} - NN_i)^2}. \quad (14)$$

If

$$d_i = NN_{i+1} - N_i, \quad (15)$$

then the standard deviation of successive differences (SDSD) is

$$\text{SDSD} = \sqrt{\frac{1}{N-1}\sum_{i=1}^{N-1}\left(d_i - \bar{d}\right)^2}, \quad (16)$$

where

$$\bar{d} = \frac{1}{N-1}\sum_{i=1}^{N-1} d_i . \quad (17)$$

The coefficient of variation of NN intervals (CVNN) is expressed as

$$\text{CVNN} = \frac{SDNN}{\overline{NN}}, \quad (18)$$

and its percentage is from

$$\text{CVNN\%} = \left(\frac{\text{SDNN}}{\overline{NN}}\right) \times 100. \quad (19)$$

The count of adjacent interval changes greater than 50ms is

$$\text{NN50} = \sum_{i=1}^{N-1} I(\,|NN_{i+1} - NN_i| > 50\,), \quad (20)$$

and the corresponding percentage is

$$\text{PNN50} = \frac{\text{NN50}}{N-1} \times 100. \quad (21)$$

Similarly, the count of adjacent interval changes greater then 20ms is

$$\text{NN20} = \sum_{i=1}^{N-1} I(\,|NN_{i+1} - NN_i| > 20), \quad (22)$$

and

$$\text{PNN20} = \frac{\text{NN20}}{N-1} \times 100. \quad (23)$$

In addition to these conventional features robust, statistical descriptors are also extracted from each segment, including the median NN interval median absolute deviation (MAD), interquartile range (IQR), and the coefficient of variation based on RMSSD:

$$\text{CVSD} = \frac{\text{RMSSD}}{\overline{NN}} \quad (24)$$

These measures improve resilience to outliers and artifact-prone beats.

2) ***Frequency-Domain HRV Features:*** For frequency domain analysis, the valid RR interval sequence is converted into an evenly sampled tachogram. Let the unevenly sampled, cubic spline interpolation is used to obtain a uniformly sampled series at 4 Hz:

$$RR_i(t) = \text{interp1}(t_{RR}, \text{RR}, t_{interp}, \text{spline}). \quad (25)$$

The interpolated sequence is then mean-centered before spectral analysis:

$$RR_c(t) = RR_i(t) - \mu_{RR_i}, \quad (26)$$

where μ_{RR_i} is the mean of the interpolated RR series.

The power spectral density (PSD) is estimated using Welch's method. If x(n) denotes the interpolated RR sequence, then its discrete spectrum is

$$X(f) = \sum_{n=0}^{N-1} x(n) e^{-j2\pi fn}, \quad (27)$$

and the corresponding PSD is

$$\text{PSD}(f) = \frac{|X(f)|^2}{N}. \quad (28)$$

The total power is defined as

$$\text{TP} = \int_0^{0.4} PDS(f)df. \quad (29)$$

The standard HRV frequency bands are calculated as

$$\text{VLF} = \int_{0.003}^{0.04} PSD(f)df, \quad (30)$$

$$\text{LF} = \int_{0.04}^{0.15} PSD(f)df, \quad (31)$$

$$\text{HF} = \int_{0.15}^{0.40} PSD(f)df. \quad (32)$$

The sympathovagal balance index is then obtained as

$$\frac{LF}{HF}. \quad (33)$$

The normalized spectral powers are computed as

$$LF_{nu} = \frac{LF}{LF+HF} \times 100, \quad (34)$$

$$HF_{nu} = \frac{HF}{LF+HF} \times 100. \quad (35)$$

*3) **Additional Spectral and Time-Frequency Analysis:*** To provide complementary spectral interpretation, the RR interval series is further analyzed using multiple spectral estimation approaches, including the classical periodogram, Welch PSD, autoregressive Burg PSD, and Lomb–Scargle periodogram. These techniques allow comparison of spectral trends under different assumptions and are particularly useful when RR interval series are short or non-uniformly sampled.

In addition, time-frequency characterization is performed using the smoothed pseudo-Wigner–Ville distribution (SPWVD). If the dedicated SPWVD function is unavailable, a spectrogram is used as a fallback representation. This step enables visualization of temporal changes in HRV spectral content and helps characterize multiscale autonomic modulation.

E. Implementation Summary

The proposed framework workflow is summarized as follows:

1) The ECG signal is loaded from the database, and the required channel for analysis is selected.

2) The signal is resampled from 250 Hz to 100 Hz to support effective peak detection.

3) Divide the ECG into 10 s segments and normalize each segment.

4) Apply the R-peak detection function to obtain intermediate processing signals, approximate peaks, and final R-peaks.

5) Convert segment-wise R-peak indices into full-record positions.

6) Compute RR intervals and reject values outside the range 0.3 s to 2 s.

7) Divide the validated peak sequence into 5 min windows for HRV analysis.

8) Extract time-domain, robust statistical, and frequency domain HRV features.

9) Analyze the spectral behavior using Welch, Burg, Lomb–Scargle, periodogram, and SPWVD-based representations.

The proposed methodology therefore combines noise resilient ECG peak detection with multiscale HRV feature extraction, enabling stable cardiac variability analysis in the presence of realistic disturbances.

IV. DATASET AND EXPERIMENT SETUP

A. Dataset Description

The proposed method was evaluated using ECG recordings from the SLP database. In the implemented workflow, the ECG signal was loaded from the database record file and the first signal channel was selected for analysis. The study considered a total of 18 ECG recordings, as reflected in the reported HRV summary tables for records such as slp01am, slp01bm, slp02am, slp02bm, slp03m, slp04m, slp14m, slp16m, slp32m, slp37m, slp41m, slp45m, slp48m, slp59m, slp60m, slp61m, slp66m, and slp67xm. These records were used to evaluate the robustness of R-peak detection and the consistency of the derived HRV parameters across multiple subjects and recording conditions.

The original ECG recordings were sampled at 250 Hz. For the R-peak detection stage, the ECG signals were resampled to 100 Hz in order to reduce computational complexity while preserving the dominant QRS morphology. The HRV analysis stage was then performed using validated R-peak annotations and RR intervals derived from the detected peaks.

B. ECG Detection Setup

For noise-resilient R-peak detection, each ECG record was processed in a segment-wise manner. The resampled signal was divided into 10 s windows, corresponding to

$$N_{seg} = f_s \times T_{seg} = 100 \times 10 = 1000 \quad (36)$$

samples per segment. Each segment was normalized using its maximum absolute amplitude prior to peak detection. This normalization reduced amplitude variability between segments and improved consistency in the filtering and decision stages. The R-peak detection algorithm was implemented using the **ecg_peakdetector_filtering** function. For each segment, the algorithm produced intermediate processing outputs

together with approximate candidate peaks and final R-peak locations. The visual outputs generated from this stage included the normalized ECG waveform, intermediate transformed signals, approximate peaks, and final detected R-peaks. These plots were used to verify the operation of the detector and to assess whether the QRS complexes were accurately preserved after preprocessing.

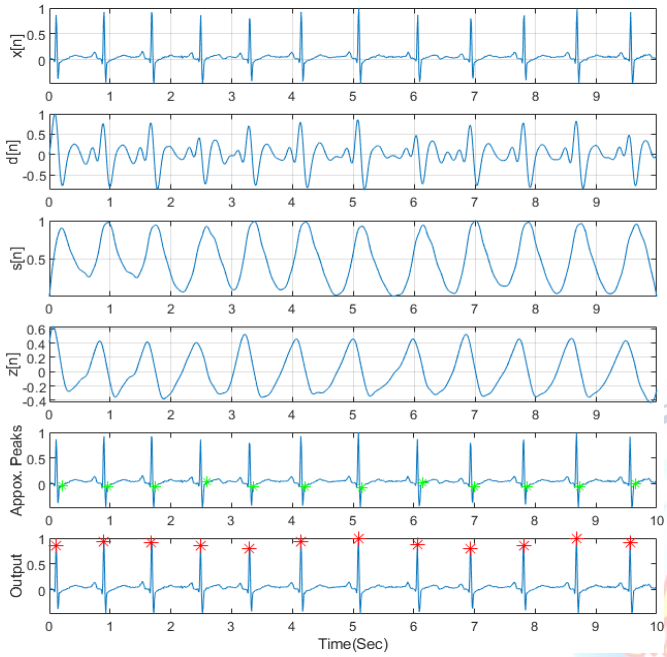

Fig. 2. Intermediate processing stages and final R-peak detection results for a representative ECG segment. The figure shows the normalized ECG, transformed detection signals, approximate candidate peaks, and refined R- peak locations.

C. HRV Analysis Setup

After R-peak detection, the detected peak positions were converted into RR intervals and screened using physiological constraints. Only intervals satisfying

$$0.3 < RR_i < 2.0 \text{ s} \quad (37)$$

were retained for HRV analysis.

This step reduced the influence of false detections, missed beats, and artifact contaminated segments.

The validated R-peak series was then analyzed using non- overlapping 5 min windows. For each window, time-domain and frequency-domain HRV parameters were computed. The time-domain analysis included conventional measures such as Mean NN, SDNN, SDSD, RMSSD, pNN50, pNN20, and Mean HR, together with robust measures including Medi- an NN, CVNN, CVSD, MAD, and IQR. The frequency-domain analysis included VLF, LF, HF, total power (TP), LF/HF ratio, and normalized spectral powers (LF_{un} and HF_{un}). These parameters were computed for all valid segments of each ECG record, and the mean ± standard deviation values were summarized across the 18 signals.

D. Spectral Estimation Setup

For frequency-domain analysis, the unevenly spaced RR interval sequence was converted into an evenly sampled tachogram using cubic spline interpolation at 4 Hz. The interpolated RR series was then mean-centered before spectral estimation. Welch's method was used to estimate the power spectral density for the primary computation of VLF, LF, HF, TP, and LF/HF.

To provide additional spectral interpretation, the study also generated comparative spectral plots using the classical periodogram, Welch periodogram, Burg autoregressive PSD, and Lomb–Scargle periodogram. These complementary methods were used to examine the spectral behavior of RR intervals under different estimation assumptions.

E. Time-Frequency Analysis Setup

To examine the temporal evolution of HRV spectral content, a time-frequency analysis was also performed. In the implemented framework, the smoothed pseudo-Wigner Ville distribution (SPWVD) was used when the required function was available. Otherwise, a spectrogram-based representation was generated as an alternative. This analysis provides a visualization of how the spectral components of RR variability changed over time and supported multiscale HRV assessment.

F. Performance Reporting

The results for each ECG record were summarized using the mean ± standard deviation. Table I represents the time-domain HRV parameters computed from the analysed SLP database records, while Table II represents the corresponding frequency-domain HRV parameters. These tables provide the numerical basis for evaluating the stability of the proposed R-peak detection and HRV estimation framework across all the 18 signals.

V. RESULTS AND DISCUSSION

The proposed noise-resilient R-peak detection framework was evaluated using 18 ECG records from the SLP database. This section discusses the accuracy of R-peak detection and the reliability of the derived HRV parameters in both time and frequency domains.

A.R-Peak Detection Performance

The proposed method processes the ECG signal in short segments and produces intermediate transformed signals be- fore finalizing the R-peak locations. As shown in Figure 2, The normalized ECG waveform, intermediate processed signals, approximate peak candidates, and final detected R-peaks indicate that the detected framework is capable of identifying the QRS complexes while suppressing unwanted disturbances. The progressive refinement from approximate candidates to final R-peaks highlights the usefulness of the multistage filtering and decision process for robust detection.

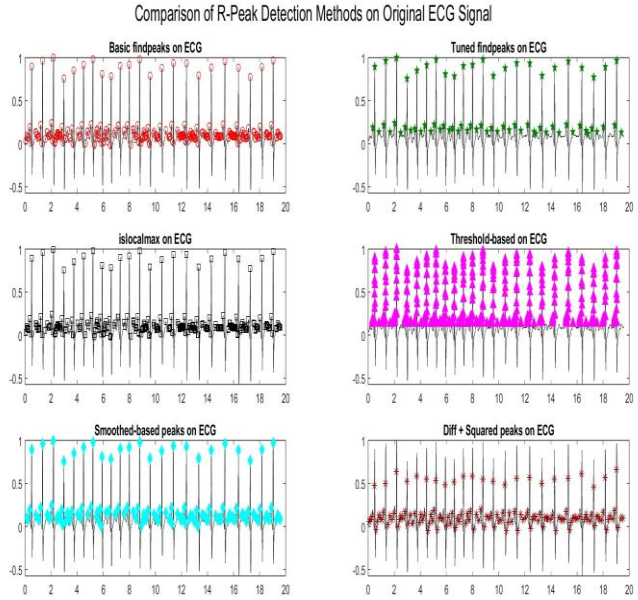

Fig. 3. Comparison of R-peak detection methods on representative ECG signals using conventional peak-finding approaches and the proposed detection framework.

The comparison results indicate that traditional methods such as findpeaks, islocalmax, and basic threshold-based approaches are more sensitive to waveform fluctuations and noise artifacts. In comparison, the proposed framework provides more consistent peak localization by combining signal enhancement, candidate selection, and physiological validation stages. This reduces false detections and improves robustness across different ECG signal conditions.

In practical ECG monitoring, especially in wearable or ambulatory conditions, signal quality is often affected by motion artifacts, amplitude variation, and baseline disturbances that affects the morphology of the QRS complex. The visual output in Fig. 2 suggests that the proposed detector maintains the dominant QRS structure and provides stable peak localization, which is essential for subsequent RR interval estimation and HRV computation.

The accurate identification of R-peaks is a critical requirement for reliable HRV analysis because even a small number of missed or falsely detected beats can significantly affect RR interval statistics and derived HRV parameters. The observed consistency of the detected peaks across different signal conditions suggests that the proposed framework provides a dependable RR interval sequence for both time-domain and frequency-domain HRV computation. This capability is particularly important when analysing long-duration recordings, where cumulative detection errors may distort autonomic nervous system assessment.

B.Time-Domain HRV Results

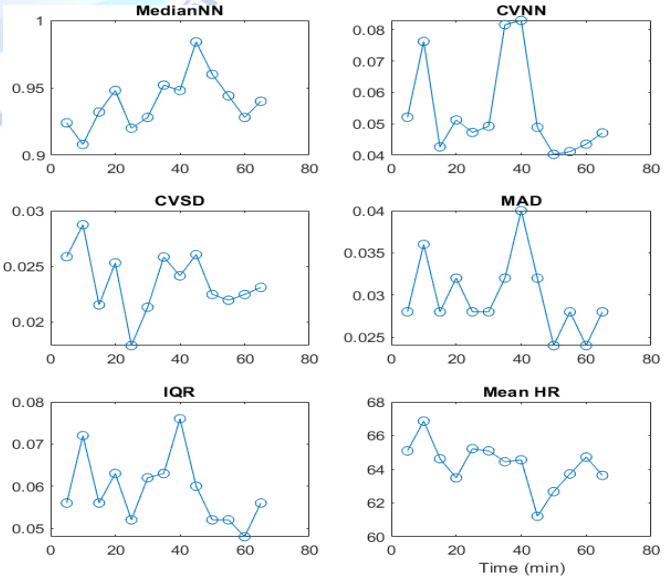

The time-domain HRV parameters derived from the detected peaks for the 18 SLP database records are listed in Table I. The results indicate that the proposed detection framework provides consistent HRV parameters from multiple recordings.

TABLE 1: TIME-DOMAIN HRV PARAMETERS (MEAN ± SD) FOR THE SLP DATABASE RECORDS.

Record	SDNN	RMSSD	CVNN	CVSD
slp01am	0.0507 ± 0.0141 s	0.0221 ± 0.0026 s	0.0542 ± 0.0154	0.0236 ± 0.0028
slp01bm	0.0519 ± 0.0207 s	0.0222 ± 0.0073 s	0.0587 ± 0.0245	0.0249 ± 0.0083
slp02am	0.0770 ± 0.0459 s	0.0757 ± 0.0467 s	0.1160 ± 0.0662	0.1137 ± 0.0660
slp02bm	0.0692 ± 0.0401 s	0.0649 ± 0.0467 s	0.0928 ± 0.0514	0.0859 ± 0.0593
slp03m	0.1189 ± 0.0139 s	0.0678 ± 0.0117 s	0.1327 ± 0.0159	0.0752 ± 0.0106
slp04m	0.0821 ± 0.0433 s	0.0591 ± 0.0356 s	0.1093 ± 0.0533	0.0785 ± 0.0444
slp14m	0.0643 ± 0.0218 s	0.0395 ± 0.0138 s	0.0680 ± 0.0231	0.0416 ± 0.0141
slp16m	0.0547 ± 0.0106 s	0.0248 ± 0.0071 s	0.0778 ± 0.0142	0.0350 ± 0.0092
slp32m	0.0574 ± 0.0242 s	0.0300 ± 0.0173 s	0.0640 ± 0.0247	0.0334 ± 0.0185
slp37m	0.0782 ± 0.0109 s	0.0349 ± 0.0072 s	0.1106 ± 0.0130	0.0493 ± 0.0090
slp41m	0.0599 ± 0.0145 s	0.0246 ± 0.0085 s	0.0713 ± 0.0180	0.0293 ± 0.0099
slp45m	0.0449 ± 0.0132 s	0.0357 ± 0.0087 s	0.0573 ± 0.0171	0.0455 ± 0.0107
slp48m	0.0905 ± 0.0136 s	0.0473 ± 0.0102 s	0.1046 ± 0.0174	0.0546 ± 0.0121
slp59m	0.0799 ± 0.0194 s	0.0411 ± 0.0110 s	0.1000 ± 0.0221	0.0515 ± 0.0122
slp60m	0.0700 ± 0.0105 s	0.0456 ± 0.0066 s	0.0862 ± 0.0122	0.0562 ± 0.0080
slp61m	0.0866 ± 0.0195 s	0.0622 ± 0.0372 s	0.1090 ± 0.0287	0.0794 ± 0.0517
slp66m	0.0963 ± 0.0146 s	0.0508 ± 0.0144 s	0.1103 ± 0.0161	0.0575 ± 0.0144
slp67xm	0.0796 ± 0.0095 s	0.0320 ± 0.0038 s	0.0923 ± 0.0119	0.0371 ± 0.0049

The SDNN values range from 0.0449 ± 0.0132 s for record slp45m to 0.1189 ± 0.0139 s for record slp03m. Similarly, RMSSD varies from 0.0221 ± 0.0026 s for slp01am to 0.0757 ± 0.0467 s for slp02am. The coefficient of variation of NN intervals (CVNN) spans from 0.0542 ± 0.0154 to 0.1327 ± 0.0159, while CVSD ranges from 0.0236 ± 0.0028 to 0.1137 ± 0.0660. These ranges indicate that the detected RR sequences maintain physiologically meaningful variations required for reliable HRV analysis.

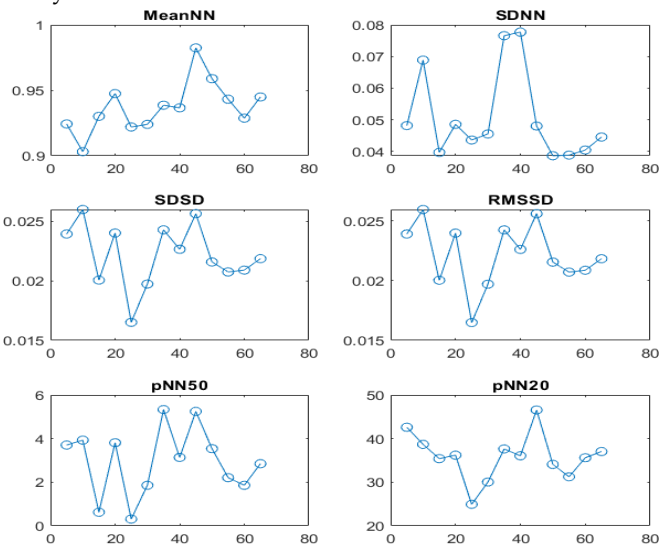

Fig. 4. Time-domain HRV trends for representative 5 min segments, showing Mean NN, SDNN, SDSD, RMSSD, pNN50, and pNN20.

The plots shown in Fig. 4 provide additional insight into the time varying behavior of the time-domain HRV features. The conventional measures, including MeanNN, SDNN, SDSD, RMSSD, pNN50, and pNN20, describe overall short-term variability of the RR intervals. The observed variations across sequential windows indicate natural physiological changes while maintaining consistent estimation across the analysed recordings.

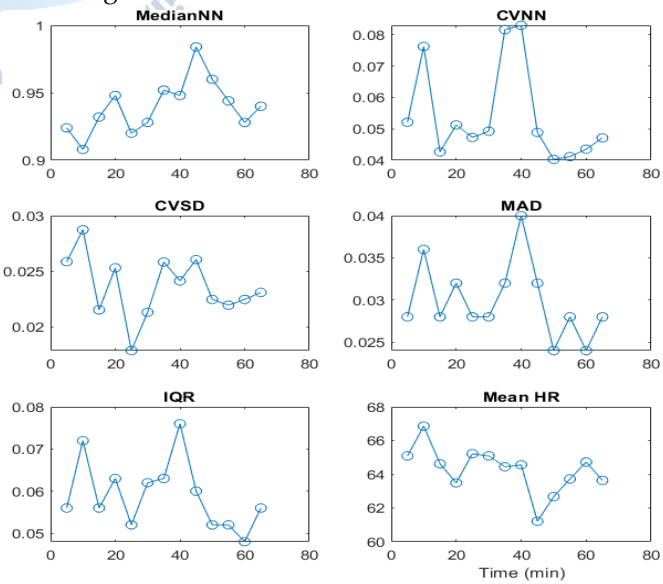

Fig. 5. Robust time-domain HRV trends for representative 5 min segments, showing Median NN, CVNN, CVSD, MAD, IQR, and Mean HR.

Fig. 5 explains about robust HRV measures that are less sensitive to outliers and occasional errors in peak detection. MedianNN, MAD, IQR, CVNN, and CVSD provide valuable information regarding the distribution and consistency of RR intervals. The stability of these parameters across multiple windows further supports the reliability of the proposed R-peak detection framework for accurate HRV analysis.

C. Frequency-Domain HRV Results

The frequency-domain HRV parameters for the same 18 ECG records are listed in Table II. These results further confirm that the proposed framework produces meaningful spectral HRV measures from the detected RR intervals.

TABLE 2: FREQUENCY-DOMAIN HRV PARAMETERS (MEAN ± SD) FOR THE SLP DATABASE RECORDS.

Record	LF	HF	TP	LF/HF
slp01am	0.0013 ± 0.0003	0.0002 ± 0.0001	0.0032 ± 0.0017	8.5696 ± 4.1934
slp01bm	0.0006 ± 0.0003	0.0003 ± 0.0002	0.0028 ± 0.0019	3.1504 ± 2.3768
slp02am	0.0036 ± 0.0034	0.0029 ± 0.0035	0.0091 ± 0.0083	1.3644 ± 0.8811
slp02bm	0.0023 ± 0.0039	0.0016 ± 0.0022	0.0071 ± 0.0112	1.4804 ± 0.5418
slp03m	0.0070 ± 0.0020	0.0015 ± 0.0006	0.0166 ± 0.0039	5.4613 ± 2.7890
slp04m	0.0052 ± 0.0051	0.0026 ± 0.0023	0.0120 ± 0.0108	2.0711 ± 0.8293
slp14m	0.0015 ± 0.0010	0.0005 ± 0.0004	0.0048 ± 0.0036	3.6559 ± 2.3654
slp16m	0.0012 ± 0.0005	0.0003 ± 0.0001	0.0035 ± 0.0013	4.7348 ± 2.1061
slp32m	0.0018 ± 0.0018	0.0003 ± 0.0003	0.0041 ± 0.0038	9.5616 ± 4.8899
slp37m	0.0036 ± 0.0015	0.0004 ± 0.0002	0.0085 ± 0.0027	9.1904 ± 1.1427
slp41m	0.0014 ± 0.0007	0.0001 ± 0.0001	0.0042 ± 0.0024	11.8765 ± 4.1753
slp45m	0.0007 ± 0.0004	0.0007 ± 0.0003	0.0023 ± 0.0015	0.9377 ± 0.5480
slp48m	0.0038 ± 0.0016	0.0006 ± 0.0002	0.0113 ± 0.0043	6.8510 ± 2.8303
slp59m	0.0029 ± 0.0020	0.0006 ± 0.0003	0.0081 ± 0.0043	4.6424 ± 2.7188
slp60m	0.0017 ± 0.0004	0.0010 ± 0.0004	0.0056 ± 0.0016	1.8535 ± 0.9275
slp61m	0.0027 ± 0.0012	0.0011 ± 0.0008	0.0076 ± 0.0028	3.2639 ± 1.8032
slp66m	0.0043 ± 0.0023	0.0011 ± 0.0005	0.0112 ± 0.0039	3.8676 ± 0.9155
slp67xm	0.0016 ± 0.0005	0.0005 ± 0.0001	0.0072 ± 0.0014	3.4879 ± 1.1327

The LF power values vary from 0.0006 ± 0.0003 for slp01bm to 0.0070 ± 0.0020 for slp03m, whereas the HF power ranges from 0.0001 ± 0.0001 for slp41m to 0.0029 ± 0.0035 for slp02am. Total power spans from 0.0023 ± 0.0015 to 0.0166 ± 0.0039, and the LF/HF ratio ranges from 0.9377 ± 0.5480 to 11.8765 ± 4.1753.

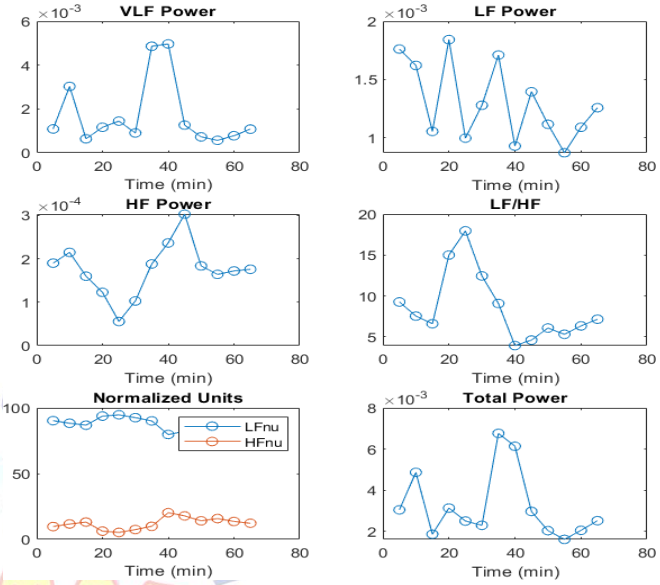

Fig. 6. Frequency-domain HRV trends for representative 5 min segments, including VLF, LF, HF, LF/HF, normalized spectral powers, and total power.

The plots in Fig. 6 show the time variation of VLF, LF, HF, LF/HF ratio, normalized spectral powers, and total power. These parameters are useful for understanding the distribution of autonomic activity over different frequency bands. The stable behavior of these estimated values across different frequencies suggests that the RR interval sequences generated by the proposed detector are suitable for accurate frequency domain HRV analysis.

D. Comparative Spectral and Time-Frequency Analysis

In order to further analyze the frequency characteristics of the extracted RR interval series, the study also generated comparative spectral plots using the classical periodogram, Welch PSD, Burg PSD, and Lomb–Scargle periodogram techniques.

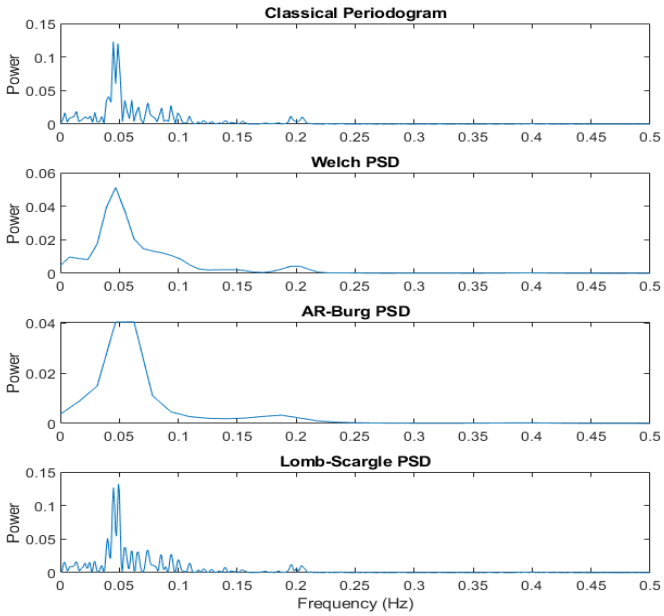

Fig. 7. Comparative spectral estimation of RR interval variability using the classical periodogram, Welch PSD, Burg PSD, and Lomb–Scargle periodogram.

Fig. 7. Explains that the applied spectral analysis techniques effectively capture the low and high frequency information contained in the RR interval series. Among them, the Welch-based PSD used for quantitative HRV estimation provides stable band power estimation, while the Lomb–Scargle method is useful for analysing non-uniform
RR interval behavior.

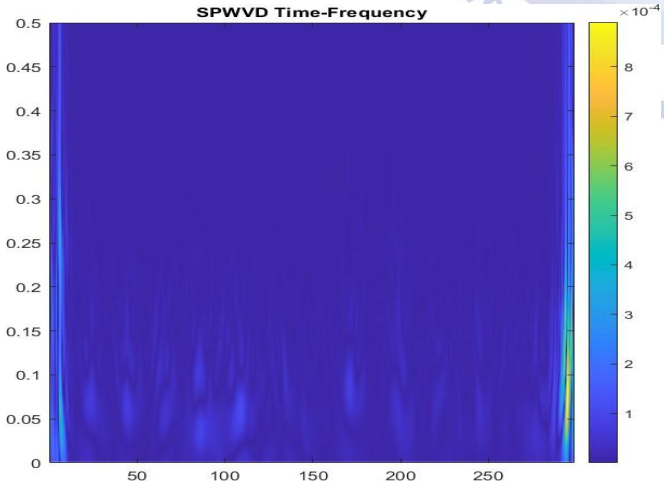

Fig. 8. Time-frequency representation of RR interval variability obtained using SPWVD or its spectrogram-based fallback.

The time-frequency representation shown in Fig. 8 provides a multiscale view of the time varying spectral energy patterns in the RR interval sequence. The use of the smoothed pseudo-Wigner Ville distribution (SPWVD), or the fallback spectrogram when SPWVD is unavailable, helps visualization of dynamic variations in autonomic nervous system activity. This representation is useful in identifying variations in spectral activity over time that may not be fully captured by a single stationary spectral estimate.

The agreement between the different spectral estimation approaches and the time frequency representation further supports the quality of the extracted RR interval sequence and supports the reliability of the proposed framework for comprehensive HRV analysis.

E. Discussion

The results indicate that the proposed framework is capable of generating reliable HRV measurements from ECG recordings after accurate R-peak detection. The time-domain parameters show consistent variability patterns across the evaluated recordings, while the frequency domain features retained important information related to autonomic nervous system activity. In addition, robust statistical measures, such as MedianNN, MAD, IQR, CVNN, and CVSD improved the analysis of HRV characteristics, mainly when the signals contained noise or artifacts. Overall, the combined findings from the peak detection plots, HRV trend figures, tabulated numerical results, and spectral representations suggests that the proposed approach is suitable for multiscale HRV analysis in realistic ECG monitoring conditions. Furthermore, the framework shows strong growth for wearable health devices and long duration ECG monitoring systems where accurate R-peak detection in the presence of signal disturbances is crucial for cardiovascular assessment.

VI. CONCLUSION

This paper presented a robust noise-resilient R-peak detection framework for multiscale heart rate variability analysis using ECG signals obtained under realistic monitoring conditions. The proposed method integrated ECG preprocessing, segment-wise peak detection, physiological validation of RR intervals, and multiscale HRV feature extraction in both time and frequency domains. To improve performance under challenging conditions, the framework was designed to improve reliability in the presence of noise, motion artifacts, and waveform distortions. The experimental evaluation on

18 records from the SLP database showed that the proposed framework produced stable and physiologically meaningful HRV estimates. In the time domain, SDNN ranged from 0.0449 ± 0.0132 s to 0.1189 ± 0.0139 s, while RMSSD varied from 0.0221 ± 0.0026 s to 0.0757 ± 0.0467 s. In the frequency domain, LF power ranged from 0.0006 ± 0.0003 to 0.0070 ± 0.0020, HF power ranged from 0.0001 ± 0.0001 to 0.0029 ± 0.0035, and the LF/HF ratio varied between 0.9377 ± 0.5480 and 11.8765 ± 4.1753. These results indicate that the detected R-peak sequences maintained meaningful variability information required for reliable HRV analysis. Overall, the proposed methodology provides a practical solution for ECG-based HRV analysis in wearable and long-term cardiac monitoring applications. As future work, the framework can be extended through large-scale validation on various ECG databases with widely used QRS detection techniques, along with adaptive algorithms for improved robustness under severe noise and arrhythmic conditions.

Conflict of interest statement

Authors declare that they do not have any conflict of interest.

REFERENCES

[1] T. N. Kipf and M. Welling, "Semi-Supervised Classification with Graph Convolutional Networks," in Proc. ICLR, 2017.

[2] L. Wen, J. Cao, Z. Zeng, Q. Cao, K. Chen, and G. Gu, "Utilizing Biomedical Radar in Clinical Doppler Cardiographic Detection of Atrial Arrhythmias," in 2025 IEEE MTT-S International Wireless Symposium (IWS), May 2025, pp. 1–3.

[3] Y. Ma, J. Zong, X. Ren, Z. Li, K. Hao, Y. Yuan, and G. Wang, "Robust AI-Driven Arrhythmia Detection via Compressive Sensing and Lightweight CNN," IEEE Internet of Things Journal, 2025.

[4] L. Zhao, R. Lyu, A. Zhou, Q. Guo, and H. Ma, "mmCG: Non-Contact Millimeter-Wave Cardiography for Heart Rate Variability Monitoring," IEEE Internet of Things Journal, 2025.

[5] A. Gupta, S. R. Devasahayam, and B. N. Subudhi, "Heart Rate and HRV Estimation Using PPG Based on Superlet Transform and LSTM Network," IEEE Transactions on Instrumentation and Measurement, 2025.

[6] T. Hasna, N. Sindhu, and K. Deepika, "Enhancing Anxiety Detection Through ECG-Derived HRV Features and Machine Learning," in 2025 6th International Conference on Control, Communication and Comput- ing (ICCC), May 2025, pp. 1–6.

[7] H. Hossam, R. Tamer, M. Mohsen, O. Ahmed, M. Alaa, J. Mourad, and S. Sherif, "ECG Stress Detection Leveraging Deep Learning Tech- niques," in 2025 Intelligent Methods, Systems, and Applications (IMSA), July 2025, pp. 407–414.

[8] N. Gao, Y. R. Li, D. Cai, and X. Y. Huang, "Dense Transformer: A Generalizable and Robust Deep Learning Method for Atrial Fibrilla- tion Prediction from Short Electrocardiogram Signals," in 2025 4thInternational Symposium on Computer Applications and Information Technology (ISCAIT), March 2025, pp. 1587–1592.

[9] A. Raimondi, A. Busacca, G. C. Giaconia, Y. Antonacci, S. Stivala, L. Faes, and R. Pernice, "Effects of Electrocardiographic Noise on Ultra- Short Term Heart Rate Variability Indices," Computers in Biology and Medicine, vol. 196, p. 110803, 2025.

[10] J. Ding, Q. Liu, B. W. K. Ling, and W. Li, "Heart Rate Estimation Based on Joint Convolutional Neural Network and Conditional Generative Adversarial Network via Heart Rate Variabilities and Other Features Extracted from Photoplethysmograms," Biomedical Signal Processing and Control, vol. 112, p. 108831, 2026.

[11] A. K. Dwivedi, A. Yadav, and R. S. Gamad, "Heart Disease Prediction using Hybrid Machine Learning with ECG Dataset for Healthcare-IOT Application," in 2025 4th OPJU International Technology Conference (OTCON) on Smart Computing for Innovation and Advancement in Industry 5.0, April 2025, pp. 1–6.

[12] X. Zhan, C. Zhou, Y. Wei, F. M. Dahlweid, H. Sun, C. Wang, B. Xie, and X. Zhang, "Estimating Heart Rate Variability Parameters in Long-Term rPPG Signals Using Spatiotemporal Attention Mechanisms," Biomedical Signal Processing and Control, vol. 112, p. 108407, 2026.

[13] C. N. Henderson, M. Smith, D. F. Johnson, and P. K. Stein, "Feasibility Considerations of 24-Hour Heart Rate Variability as a Wellness-Focused Biomarker," Journal of Chiropractic Medicine, vol. 24, no. 1–4, pp. 54– 61, 2025.

[14] X. Tang and R. He, "Association Between Ultra-Short-Term Heart Rate Variability and Atrial Fibrillation in Heart Failure Population: A Retrospective Cohort Study," Heart, Lung and Circulation, 2025.

[15] M. A. Bennet, R. Remya, J. J. P. Glora, T. D. Kumar, and R. Selvakani, "A Hybrid AI Framework with Automatic Gain Control for Real-Time ECG Signal Monitoring," in 2025 International Conference on Next Generation Computing Systems (ICNGCS), August 2025, pp. 1–8.

[16] R. Tamezheneal, B. Sathiyaprasad, M. G. Vivitha, R. N. Gopika, S. Velan, and A. Yaswanth, "A Hybrid Deep Learning and Statistical Framework for Cardiac Arrest Detection in Neonatal Intensive Care Units," in 2025 International Conference on Computing and Communi- cation Technologies (ICCCT), April 2025, pp. 1–7.

[17] H. Shan and W. Jin, "A Multi-Sensor-Based System for Cardiovascular Health Monitoring," in 2025 5th International Conference on Sensors and Information Technology, March 2025, pp. 442–447.

[18] V. Ahuja, A. Dhiman, J. Kaur, V. Jain, and L. Singla, "A Performance- Driven Hybrid CNN-RF Model for Arrhythmia Detection: Insights Ap- proach," in 2025 6th International Conference for Emerging Technology (INCET), May 2025, pp. 1–6.

[19] R. Mohith, B. Sharmila, and C. Saraswathy, "Advanced Deep Learning Approaches for Automated Diagnosis of Cardiac Arrhythmia in Multi- lead ECG Signals," in 2025 IEEE Open Conference of Electrical, Electronic and Information Sciences (eStream), April 2025, pp. 1–5.

[20] S. Yadav, R. Gupta, and R. Bajaj, "An Optimised Model for Arrhythmia Prediction using FSM," in 2025 International

Conference on Computa- tional Robotics, Testing and Engineering Evaluation (ICCRTEE), May 2025, pp. 1–7.

[21] P. E. MT, G. Soysal, O. Erog˘ul, and S. Yetkin, "Detection of Panic At- tacks Using Convolutional Neural Networks on ECG Data," in 2025 7th International Congress on Human-Computer Interaction, Optimization and Robotic Applications (ICHORA), May 2025, pp. 1–6.

[22] K. Viswateja, D. Supriya, K. B. Jahnavi, and V. B. K. L. Aruna, "Enhanced Feature Selection Technique Using Machine Learning Algo- rithm for Accurate Heart Disease Classification," in 2025 International Conference on Computing Technologies (ICOCT), June 2025, pp. 1–6.

[23] A. Tripathi and S. Ayub, "Heart Rate Variability Detection in Arrhyth- mia," in 2015 International Conference on Computational Intelligence and Communication Networks (CICN), December 2015, pp. 357–362.

[24] M. C. Singh, V. Priya, K. A. Kumar, A. Aravind, C. Bhavani, P. S. Kumar, and B. Venkataramanaiah, "Impulsive Cardiac Death Prediction Model Using Machine Learning and Deep Learning Techniques," in 2025 International Conference on Data Science, Agents & Artificial Intelligence (ICDSAAI), March 2025, pp. 1–7.

[25] F. Zhou, Y. Wang, and Y. Sun, "Inter-Patient ECG Arrhythmia Heartbeat Classification Method Based on Task Fusion and Rule Inference," in 2025 IEEE 8th International Conference on Signal Processing and Machine Learning (SPML), July 2025, pp. 1–8.

[26] K. Sathya and G. Magesh, "Multimodal Deep Learning for Cardiovascu- lar Risk Stratification: Integrating Retinal Biomarkers and Cardiovascu- lar Signals for Enhanced Heart Attack Prediction," IEEE Access, 2025.

International Journal for Modern Trends in Science and Technology
IJMTST